UNIVERSITY OF CALIFORNIA, SAN DIEGO
SCRIPPS INSTITUTION OF OCEANOGRAPHY
VISIBILITY LABORATORY
SAN DIEGO, CALIFORNIA 92152

IMAGE INTENSIFIER SYSTEM DETECTION EXPERIMENT

Richard L. Ensminger, Robert F. Howarth, Alma L. Shaules

SIO Ref. 72-60

June 1972

U. S. Naval Ship Systems Command

Department of the Navy

Contract N00024-68-C-1100

Approved:

S. Q. Duntley

Seibert Q. Duntley, Director
Visibility Laboratory

Approved for Distribution:

William A. Nierenberg, Director
Scripps Institution of Oceanography

ABSTRACT

This report describes experiments to evaluate the efficiency of human information extraction from an image intensifier system. A detection experiment was run with circular targets. The variables of the experiment were the angular size of the targets and the contrast of the targets. The experimental data are compared with calculations of the performance that would be achieved if the observer extracted all information collected by the image intensifier system.

Contents

1. INTRODUCTION

In recent years improved image intensifier tubes have been incorporated in low-light-level devices, such as the U. S. Army's Starlight Scope. This equipment has resulted in greatly increased nighttime capabilities for many important operations. With such a breakthrough it is quite natural to want to follow the original success with research and development effort directed toward further exploitation of this equipment concept.

If the yield from such R & D effort is to be maximized, attempts should be made to determine the potential performance gains achievable by various types of system improvements and to weigh these performance gains against the cost and probability of success of the required R & D effort.

For any light-sensing system, fundamental performance limitations are set by the statistical nature of light. This report describes studies in which experimentally determined performance of an observer using a Starlight Scope is compared with the theoretical limit of such performance. The result is a quantitative evaluation of the efficiency of the present man/device combination in performing simple detection tasks. The data therefore give a quantitative measure of the potential performance improvement achievable if the various inefficiencies of the man/device system can be pinpointed and eliminated.

2. DESCRIPTION OF THE EXPERIMENT

2.1 GENERAL

Figure 2-1 is a sketch showing the experimental setup. These rooms are in an existing facility of the Visibility Laboratory's Vision Research Branch. The observer is seated in a chair, on the arm of which is mounted a set of response buttons. He looks into the eyepiece of a Starlight Scope* which is focused upon a uniform background (the partition on the left side of the target projector). The background illuminators indicated in the sketch are mounted around the edge of a large hole in the partition. The rear screen projection system shown on the right of the sketch allows a circular patch of light to be added to the uniform background. The control room on the left contains equipment which programs the rear screen projector and is associated with the automatic recording of observer responses.

It is mandatory in an experiment of this type that the photometric measurements of both background and target be properly made.†

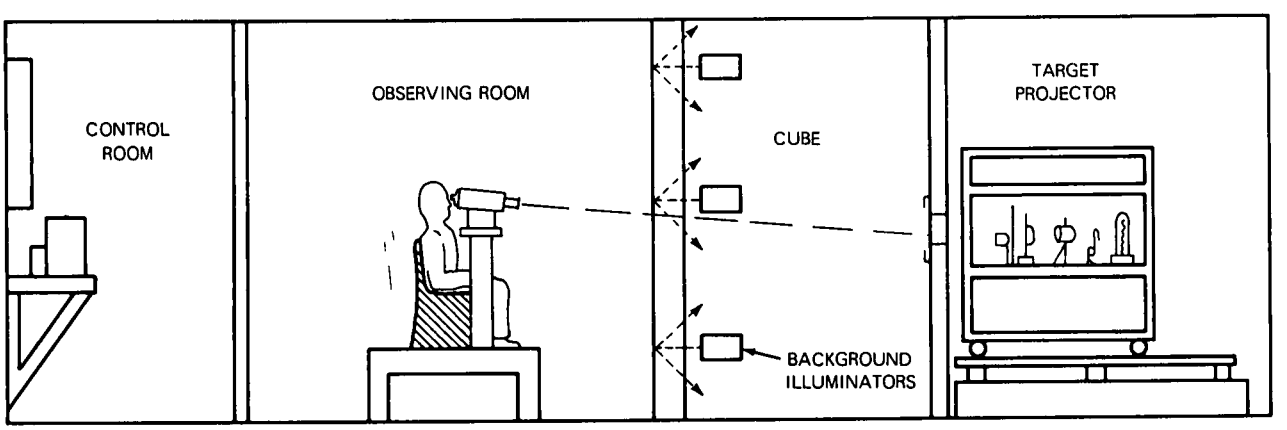

Fig. 2-1. Experimental rooms, showing control room containing automatic presentation and recording equipment, observing room for four subjects, flux integrating Cube for producing a uniform background luminance, and projection room for generation of transilluminated targets.

* The properties of the Starlight Scope appear in Appendix A.

† A detailed description of this photometer is contained in Appendix B.

2.2 EXPERIMENTAL TECHNIQUE

A procedure known as the forced-choice technique[1,2] was used in these experiments. In this technique a buzzer marks off four equal time intervals, each 2 seconds in duration. The circular target is projected on the screen during one of these time intervals with the choice of interval derived from a random number set. Only background is presented during the other three intervals. The observer has four response buttons, one for each time interval. At the conclusion of the four time intervals the observer responds by pushing one of the buttons indicating his judgment as to the time interval in which the target was presented. The technique is termed forced choice because the observer is not allowed the option of saying, "I don't know." He must indicate one of the four intervals even if he believes the choice is a total guess.

A single four-time-interval sequence constitutes one trial and requires one observer response. Fifty such trials were made for a fixed target size and contrast. The number of correct responses divided by fifty is the probability of correct decision for that target size and contrast.

Contrast was then changed, leaving target size fixed, and another set of fifty trials recorded. In all, five such contrast values were chosen to cover a range of probability of correct decision from 0.25 (chance) to 1.0 (certainty). The entire process was repeated for a range of target sizes.

The resulting experimental curves were based on the performance of one observer practiced in experiments involving a variety of visual tasks, particularly temporal detection forced choice. His vision was emmetropic.

3. EXPERIMENTAL RESULTS AND CONCLUSIONS

3.1 DATA REDUCTION

Figure 3-1 shows the experimental results. The dashed lines are normal ogive fits to the data using a technique known as fractile analysis.[3,4] From these analytic fits the contrast values which yield 0.5 probability of correct decision (liminal threshold) are determined. These liminal threshold contrast values are plotted as a function of the target size in the Fig. 3-2 curve labeled Starlight Scope. The target size is specified in terms of the angle (minutes of arc) subtended by the circular target when viewed from the entrance pupil of the Starlight Scope.

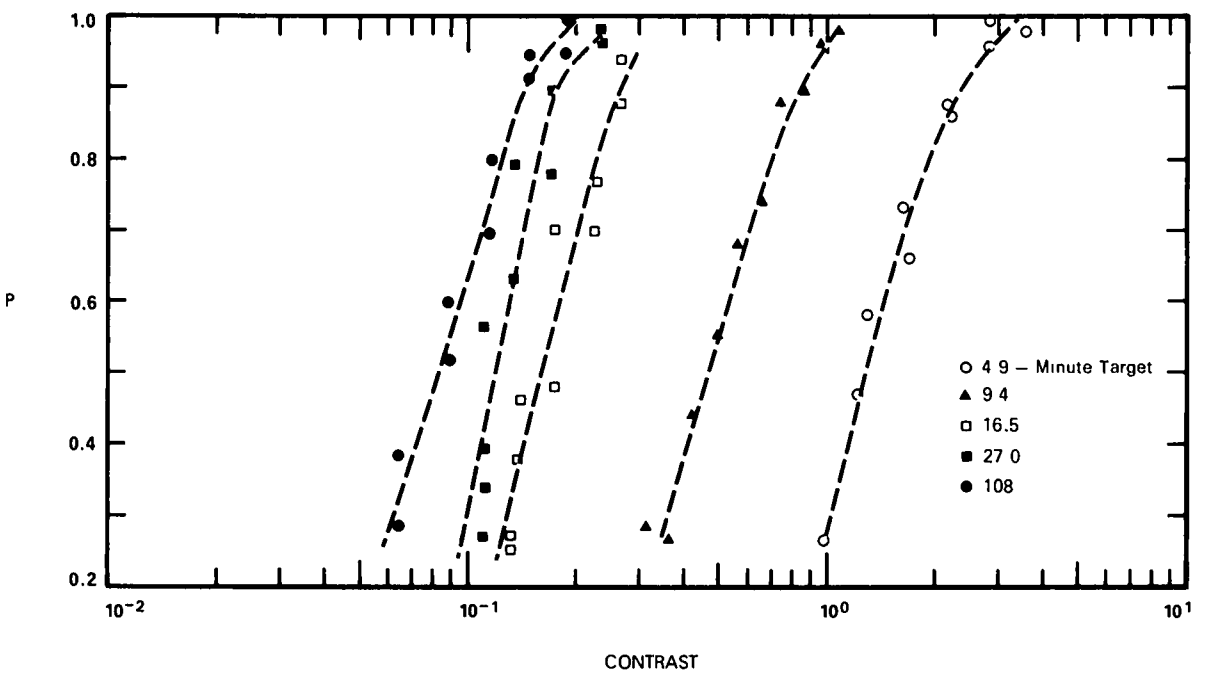

Fig. 3-1. Psychophysics Results for One Observer.

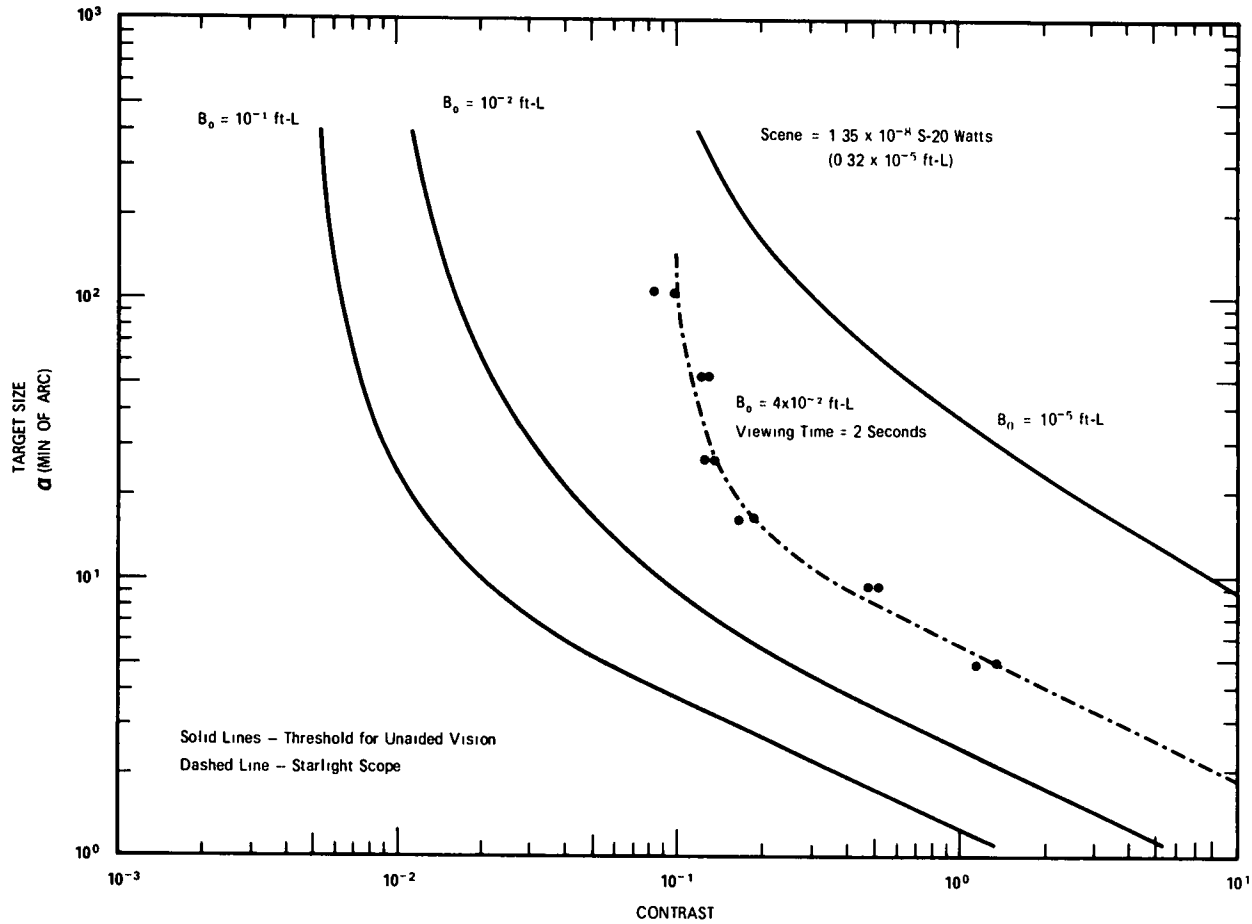

Fig. 3-2. Threshold Performance for Detection Experiment.

3.2 STARLIGHT SCOPE VERSUS UNAIDED VISION

It is a matter of interest to determine the extent to which observer performance was improved by the use of the Starlight Scope over what his performance would have been with unaided vision. A considerable body of data exists which relates contrast threshold for unaided vision as a function of the angular subtense of circular targets for a wide range of adaptation levels.[5] The right-hand curve of Fig. 3-2 is taken from these data for an adaptation level of 10^{-5} foot-lamberts. A comparison of this curve and the Starlight Scope curve shows the performance improvement furnished by the Starlight Scope. For a target whose angular subtense is 10 minutes of arc or less, the contrast threshold was decreased by approximately 25 to 1. Another way of interpreting the result is to note that for the case of unaided vision at 10^{-5} foot-lamberts, 10 minutes of arc targets would require contrasts in excess of 10 to be detectable. Such contrasts are rare in any natural scene. Therefore the Starlight Scope used in this experiment certainly represented a significant improvement over unaided vision.

It is curious, however, that this substantial improvement does not exist for large angular subtense targets. The Starlight Scope curve is suggestive of a contrast threshold asymptote of about 0.08 such that no further reduction in threshold exists with increasing angular subtense. Speculation on the causes of this behavior will be made later in this report.

3.3 LUMINANCE ENHANCEMENT

If the image intensifier were a perfect device and if photon-shot-noise did not exist, the scene presented to the observer would be identical with the true scene with one exception. The luminance of all points of the scene would be multiplied by the luminance or brightness gain of the tube. Under these conditions observer performance could be determined by examining the contrast threshold data for unaided vision at an adaptation level equal to the image intensifier output-phosphor luminance level.

For the experiment described in this report, the true scene luminance was 0.32×10^{-5} foot-lamberts. The phosphor screen had a luminance of 4×10^{-2} foot-lamberts. Therefore the luminance gain of the tube was 1.25×10^{4}. Two unaided vision threshold curves labeled 10^{-1} and 10^{-2} foot-lamberts are shown on the left of Fig. 3-2.

A comparison of these curves with the Starlight Scope curve shows that the Starlight Scope does not live up to the performance expected from a perfect noise-free luminance enhancement device. This result is in no way surprising since the Starlight Scope is not a perfect device and the granularity of light, i.e., photon structure, introduces a limiting noise.

3.4 THE CONCEPT OF THE IDEAL DETECTOR

Light is transmitted in discrete energy bundles called photons. The number of photons emitted or reflected from any object during a specified period of time is a statistical quantity. When the luminance or radiance of an object is specified, it is implied that this refers to a longtime average.

This statistical nature of light imposes a fundamental limitation on any light-sensing device. For example, consider two objects of almost equal luminance. In any finite measuring interval there is a finite probability that an optical system may receive an equal number of photons from the objects or that more photons may actually be received from the "darker" object. Within the framework of the present understanding of the laws of physics, this is considered to be a fundamental limitation. An image intensifier system operates in the presence of this fundamental limitation.

For a detection experiment of the type described in this report, an ideal detector would be a system which counts the number of photons received from the region of object space corresponding to the circular target, for each of the four time intervals, and decides in favor of the interval having the largest count.*

The average number of photons received at the photocathode of an image intensifier tube from any point in object space is dependent upon the inherent radiance of that point, the transmission properties of the intervening atmosphere, the size of the collecting lens, and the transmission properties of that lens.

* A detailed derivation of the equations for an ideal detector are presented in Appendix C. The present section is limited to a nonmathematical discussion of the meaning of these equations.

Using the equations from Appendix C, the performance of the ideal detector is shown in Fig. 3-3 for the lens associated with the Starlight Scope and for the viewing conditions associated with the experiment described in this report. By drawing a horizontal line at the 0.5 probability point, liminal contrast threshold can be read as a function of the angular subtense of the target. The far left-hand curve of Fig. 3-4 shows the results. The far right-hand curve is the same experimental Starlight Scope curve shown in Fig. 3-2. A comparison of these two curves shows that the observer using the Starlight Scope has a performance level considerably below that theoretically achievable.

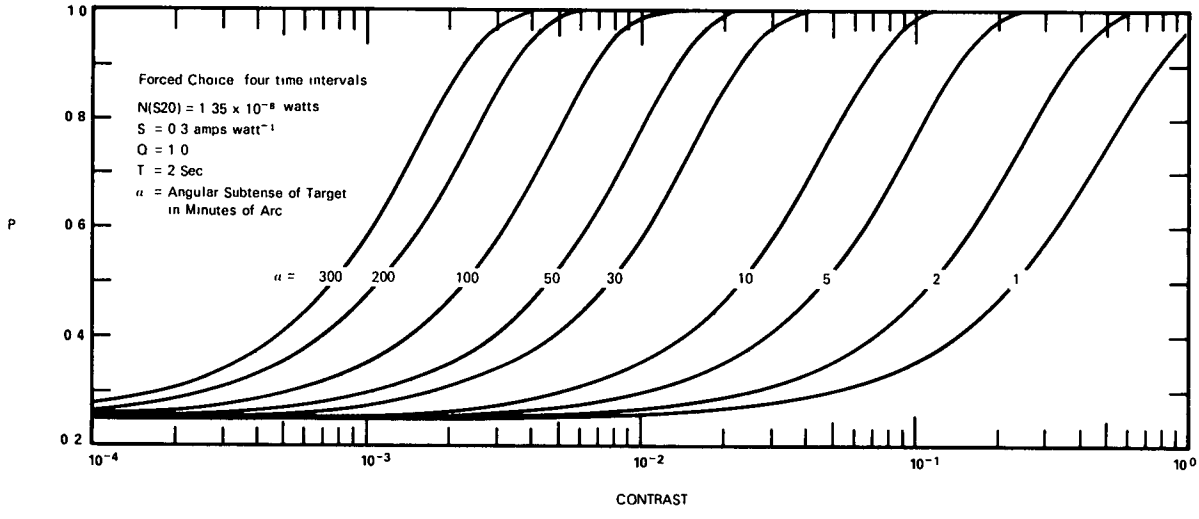

Fig. 3-3. Probability of Correct Decision by Ideal Detector.

The Q=1 label on the left-hand curve of Fig. 3-4 means that the quantum efficiency is unity, i.e., every photon which reaches the photocathode of the image intensifier is converted to an electron. Physically realizable photocathodes have quantum efficiencies more on the order of 20 percent. The performance of an ideal detector with Q=0.2 is also shown in Fig. 3-4. For an angular subtense of approximately 20 minutes of arc the Starlight Scope curve has a contrast threshold approximately five times the contrast threshold for the ideal detector. It is important to note that for angular subtense values either above or below 10 minutes of arc the ratio becomes even higher, i.e., observer performance becomes poorer relative to ideal observer performance.

It can be seen in Fig. 3-4 that the Starlight Scope curve reaches a slope of 0.5 for small angular subtense targets. This slope means that the product of contrast and the square of the angular subtense is a constant, i.e., total power from the target is a constant. This region could be properly named the region of the unresolved target. This region is exhibited by all detectors including the human eye. It simply means that when the angular size of the target drops well below the resolution capability of the system, the size or shape of the target is no longer of significance and detectability is dictated only by the total power received from the target.

If the ideal detector is modified to incorporate a resolution limit like that of the Starlight Scope, it also will exhibit the slope of 0.5. A Gaussian transfer function chosen to match the Starlight Scope modulation transfer function was added to the ideal detector calculation and the results are shown in Fig. 3-4. With this modification of the ideal observer calculation, there is now a constant ratio between contrast thresholds for the Starlight Scope and ideal observer curves once the unresolved target region is reached.

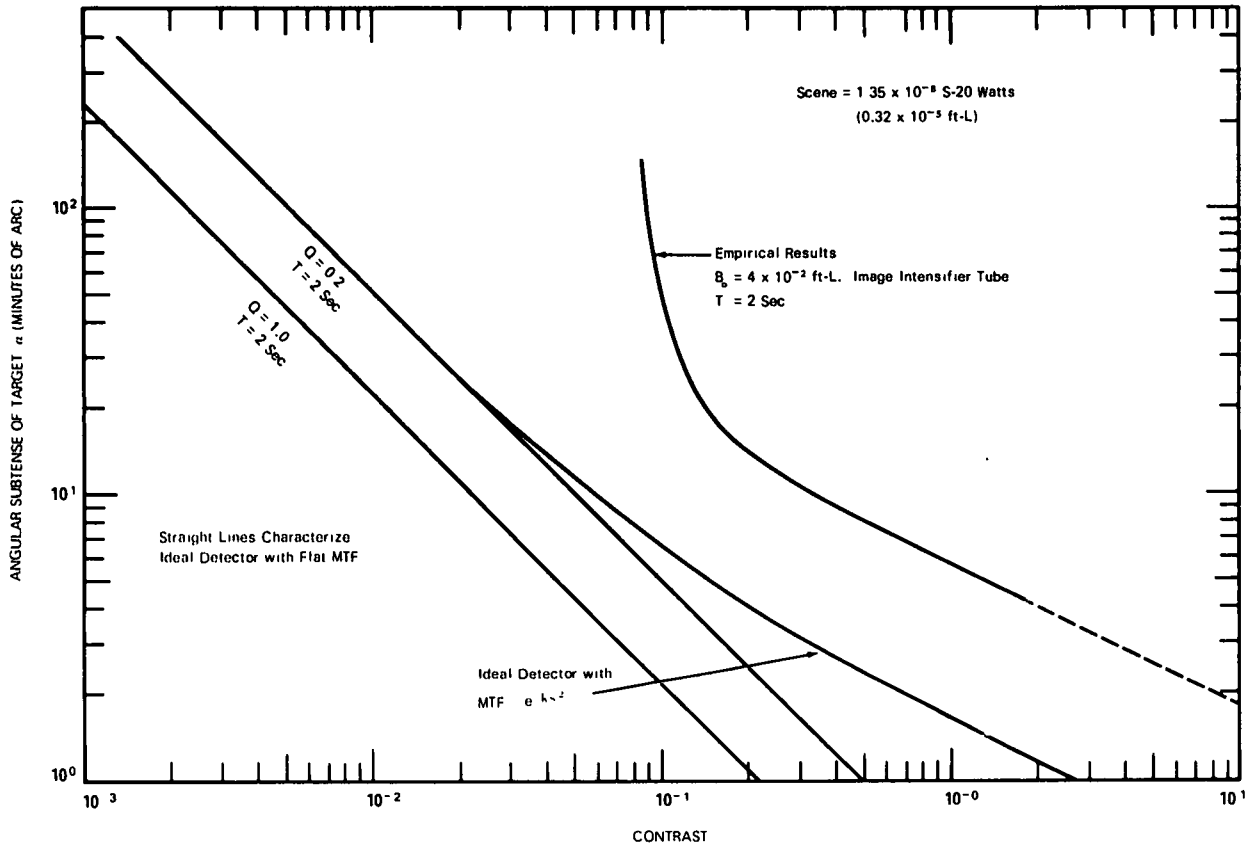

Fig. 3-4. Liminal Probability of Correct Decision.

4. CONCLUSIONS

This report has described the results of a detection experiment where an observer using a Starlight Scope is required to specify which of four 2-second time intervals contains a target. A comparison of these results with corresponding curves generated for the "ideal observer" shows that the combination of man and Starlight Scope does not produce a performance approaching the fundamental limit. The margin between the two performance levels is sufficient to warrant serious consideration of means by which the fundamental limit can be achieved. As a result of these experiments the following specific items are now receiving study.

4.1 TEMPORAL INTEGRATION

Examination of basic vision threshold data shows that the human visual system does not have the capability for performing integration in the time required to achieve ideal detector performance. It might be expected, therefore, that performance improvement could be achieved by assisting the observer in performing temporal integration. Possible approaches could include the use of long persistence phosphors or storage tube technology. It would seem desirable to have temporal integration introduced in such a way that it is adjustable, since there would certainly be occasions when the dynamics of the viewing situation would not permit longtime integration.

4.2 RESOLUTION IMPROVEMENTS

The ideal detector calculations shown in Fig. 3-4 suggest the nature of the improvement in performance which might result from increased resolution in the image intensifier tube. In the "resolved" region the contrast threshold is inversely proportional to the linear dimensions of the target. In the "unresolved" region the contrast threshold is inversely proportional to the square of the linear dimensions of the target. For the case of the ideal detector an improvement in resolution of the device means that the contrast threshold will continue along the straight line of slope equals 1.0, breaking into the slope of 0.5 at some smaller angular subtense. It should be recognized that this yields performance improvement even in the "unresolved" region. It must be remembered, however, that as the tube resolution is increased, a point will be reached where the overall resolution of the system will be determined by the human eye rather than by the image intensifier.

While it is clear what improved tube resolution would do for the ideal observer, it is much less certain what would happen with the human observer. In very noisy situations it is entirely possible that observer performance may decrease with increased system resolution for targets which are well resolved, i.e., it may be that the human visual system welcomes the spatial integration associated with a resolution limitation. For example, the experimental curve for the Starlight Scope shows maximum efficiency with respect to the ideal observer at the point of transition from resolved to unresolved targets. It is possible, therefore, that a resolution improvement in the tube might result in improvement in performance for just-resolved and unresolved targets but in a decrease in performance for well-resolved targets. Further experimental evidence is required in order to answer this question. Performance might be improved for large targets by incorporating variable spatial integration in the system such that the observer is always able to set system resolution so that the scene detail size of interest at that moment is just-resolvable.

4.3 SPURIOUS BACKGROUND DETAIL

It was pointed out earlier in connection with Fig. 3-2 that the Starlight Scope performance curve exhibits an asymptotic behavior of contrast threshold for large angular subtense targets. The asymptote appears to be approached much more rapidly than occurs in the basic vision data. This is suggestive that there is some defect in the Starlight Scope system which prevents efficient operation with large angular subtense, low contrast targets. Speculation as to the cause for this might include adverse effects due to the mottled pattern visible in the display attributable to the fiber optics coupling stages. It may be that this breakup of the uniform background makes it difficult to see low contrast detail. Techniques for eliminating this structure can be devised. Before doing so, however, it would be well to perform some basic experiments using simulated noisy imagery with and without such structure present to determine whether the structure does explain the observed performance degradation.

APPENDIX A. THE STARLIGHT SCOPE

The function of the image intensifier tube is to amplify small quantities of electromagnetic energy so that their effects may be either viewed directly by eye at photopic light levels or recorded on photographic film. The wavelength of the incident electromagnetic energy must be within the limits of the spectral sensitivity characteristic of the image intensifier's photocathode in order for amplification to take place.

Figure A-1 shows a diagram of a typical three-stage image intensifier tube of the type used in the current work. Light from an object is imaged by the objective lens onto the fiber optic faceplate of stage 1 of the intensifier. The fibers transmit the light to the first photosensitive surface where a number of photoelectrons proportional to the incident light are emitted. These photoelectrons are accelerated to the phosphor P1 by a 15 000-volt potential and electrostatically focused en route. Upon impact at P1 the high energy of the accelerated electrons is transferred to that surface causing phosphorescence. Again the fiber optics transmit the emitted phosphor energy to the next photocathode and the process is repeated for both stages 2 and 3. The output image on P3 is magnified seven times by the eyepiece and presented to the observer.

The three stages are essentially identical, each having a light gain in the range of 30 to 50. A battery-operated 1-kiloHertz inverter oscillator supplies about 2.6 kilovolts to a multiplier circuit encapsulated in the case of the image intensifier system. This multiplier outputs 45 000 volts to a resistive voltage divider which is tapped at appropriate intervals to supply the accelerating and focusing potentials needed. The Starlight Scope has all of the above features and is completely self-contained.

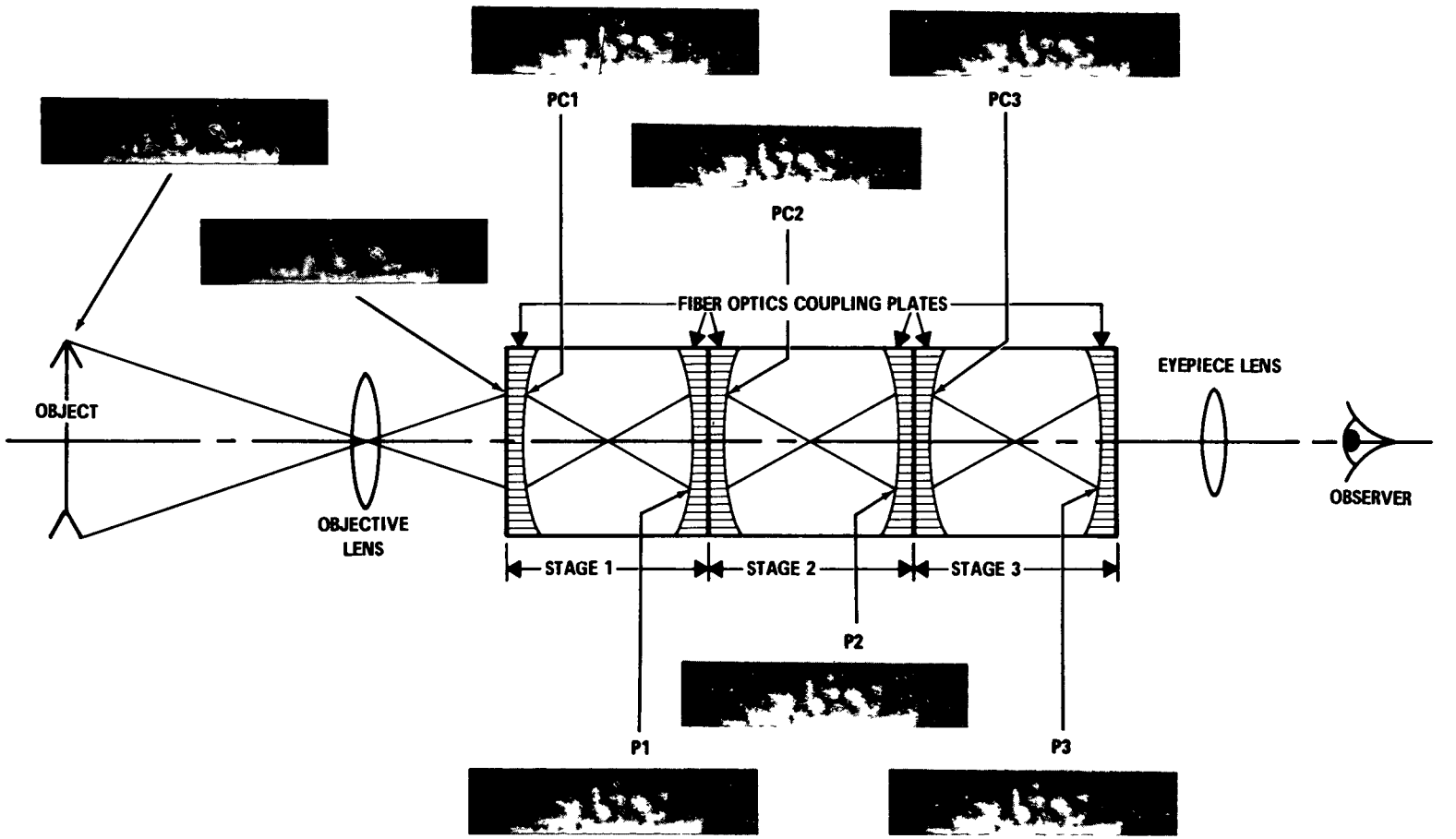

Fig. A-1. Typical Three-Stage Image Intensifier

Specifications of the Starlight Scope are as follows.*

Type:

Machlett ML-8606

Photocathode:

Diameter: 40 millimeters

Spectral Sensitivity: S-20 extended red

Display Screen:

Diameter: 40 millimeters

Phosphor: P-20, aluminized

Resolution (minimum):

90 percent MTF at 2.5 line pairs per millimeter

55 percent MTF at 7.5 line pairs per millimeter

10 percent MTF at 16.0 line pairs per millimeter

Center resolution $\geq$ 25 line pairs per millimeter

Luminance Gain:

$G \geq 35\,000$ with an input radiation of not less than 2.5×10^{-5} lm ft^{-2} (ft-c)

Maximum Output Luminance:

$\leq$ 32 lm ft^{-2} sr^{-1} (100 ft-L)

Equivalent Background Input:

Not to exceed 2×10^{-11} lm cm^{-2}

Objective Lens:

Bausch and Lomb Baltar, f/2.3, 50 millimeters

Eyepiece:

Erfle, 37 millimeters, 60-degree field

Power Source:

45 000-volt dc high voltage multiplier module requiring 2700 volts at 1200 to 2000 Hertz; primary source 7.5-volt mercury cell

* See MIL-I-55493 (EL) for complete specifications.

APPENDIX B. PHOTOMETRY AND RADIOMETRY

B.1 SCENE LUMINANCE

The scene luminance was measured by means of a Macbeth illuminometer set at a photopic level (luminance $\geq 10^{-2}$ lm ft^{-2} sr^{-1}) and then attenuated to the desired 0.32×10^{-5} lm ft^{-2} sr^{-1} (1×10^{-5} ft-L) by inserting Wratten No. 96 neutral density filters at the illuminating sources (see Fig. 2-1). All enclosing surfaces of the uniform brightness cube (Cube) were painted with a flat high-reflectance white paint to uniformly distribute the light from the illuminators over the scene region. A uniformity of ±5 percent was achieved in this manner. The measured value of 0.32×10^{-5} lm ft^{-2} sr^{-1} was accurate within ±10 percent. The illuminator lamps and the target projector lamp were operated from ac line stabilizers; stability of the background luminance was within ±5 percent as determined from daily readings.

B.2 PHOSPHOR LUMINANCE

The output phosphor luminance was measured using a Gamma Scientific model 721 photometer with fiber optics probe. This luminance was $4/\pi \times 10^{-2}$ lm ft^{-2} sr^{-1} (4×10^{-2} ft-L) and was essentially constant over the duration of a normal viewing session (20 minutes). This is the luminance level to which the viewing eye of the observer was adapted. The other eye was adapted to the much lower scene luminance. Tests made on three different occasions showed the phosphor luminance to be constant within ±2 percent over every 20-minute period.

B.3 SCENE RADIANCE

It is the scene radiance reimaged on the image intensifier photocathode that gives rise to the photoelectron current in the intensifier tube. The effective S-20 radiance was determined to be 1.35×10^{-8} W ft^{-2} sr^{-1} by comparing the image intensifier output, when viewing Cube scene, to its output when viewing a known standard lamp source. In both cases the Gamma 721 photometer head was attached to the intensifier case and used to measure the phosphor radiance. A complete description with computations can be found later in this appendix.

B.4 TARGET CONTRAST

Due to the characteristic red leakage of the Wratten No. 96 neutral density filters, it was not possible to determine target contrast by means of the usual photopic method.[6] Ordinarily, photometric measurements of both the background and unattenuated target are made first, followed by the calculation of any experimental contrast, since the transmittance factors of subsequently inserted neutral density filters are known. This, in effect, yields a photopic contrast. However, the S-20 photosensitive surface of the image intensifier is responsive to radiation beyond the photopic region so it is not photopic contrast that the intensifier "sees."

The target contrast as seen by the image intensifier was measured by means of the image intensifier itself. The Gamma photometer head was coupled to the intensifier output and measurements were made of the phosphor radiance for all difficulty levels used in the experiment and for the scene background level. In all cases the target area or the background area, depending on which was being measured, completely filled the field of view of the intensifier objective lens. Of course it was necessary to reduce the distance between the Cube screen and the intensifier when making the target measurement.

B.5 DETERMINATION OF SCENE RADIANCE

As stated earlier it is the effective S-20 watts which gives rise to the photocathode current. The effective S-20 watts is that portion of the incident photocathode irradiance which is converted to photoelectron current by the responsivity of the S-20 photocathode.

Assuming that all radiant power collected by the image intensifier's objective lens is transmitted to the photocathode, we have

$$W(S20) = \Omega_{II} A_L N_w \int_0^\infty n(\lambda) \cdot \sigma(\lambda)\, d\lambda \text{ (watts)}, \tag{B.1}$$

where:

Ω_{II} = solid angle of the objective lens field of view (steradians)

A_L = area of the objective lens (square feet)

N_w = peak value of $n(\lambda)$ (watts/square foot/steradian/nanometer)

$n(\lambda)$ = normalized spectral characteristic of scene radiance (no units)

$\sigma(\lambda)$ = normalized spectral characteristic (responsivity) of photocathode (no units).

Assume that a phototube sensitive to the phosphor radiance is attached to the phosphor end of the image intensifier housing. In this experiment the Gamma 721 telephotometer was so attached. Now when the image intensifier is focused on the Cube wall with only background radiance present, one obtains a reading of i_{cw} amperes on the telephotometer. From Eq. (B.1) we see that

$$i_{cw} = g S_{20} \cdot W(S20) \text{ (amperes)} , \tag{B.2}$$

where:

g = a measurement constant relating the telephotometer indication to the S-20 photocathode current

S_{20} = peak value of the photocathode spectral characteristic $\sigma(\lambda)$ (amperes/watt).

Hence we have a relative telephotometer indication of i_{cw} that is proportional to the unknown desired quantity W(S20) watts.

To continue the determination of the scene radiance it is necessary to calibrate the intensifier/phototube package. Consider a known tertiary standard lamp mounted on an optical bar as shown in Fig. B-1. A magnesium oxide plaque is set up at the far end of the bar and the intensifier/phototube package is adjusted so that its optical axis is 45 degrees to the bar axis and its field of view is overfilled with the plaque.

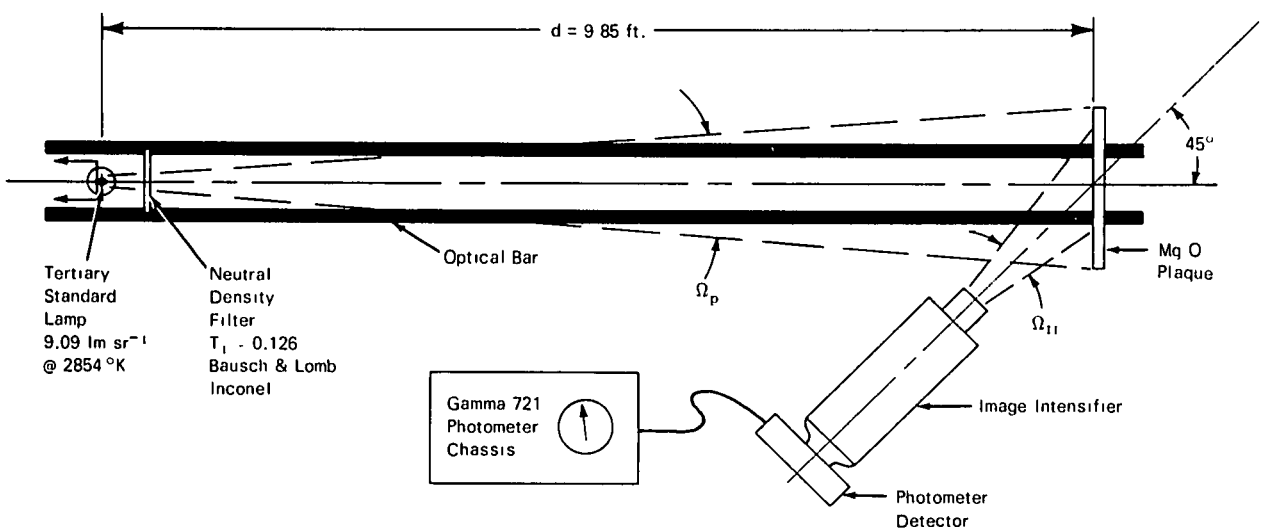

Fig. B-1. Calibration Setup for Image Intensifier/Phototube Package.

The lumen output of the lamp is

$$TI = 680\, J_p \int_0^\infty \bar{y}(\lambda) \cdot w(\lambda)\, d\lambda \text{ (lumens/steradian)} . \tag{B.3}$$

Here

T = transmittance of the neutral density filter (no units)

I = lamp intensity (lumens/steradian)

$\bar{y}(\lambda)$ = normalized eye response (no units)

680 = maximum luminous efficiency of the eye (lumens/watt)

$w(\lambda)$ = normalized spectral characteristic of lamp intensity (2870K) (no units)

J_p = peak value of $w(\lambda)$ (watts/steradian/nanometer).

Now the irradiance H, watts foot^{-2}, on the plaque is

$$H = \Omega_p \cdot \frac{1}{A_p} \cdot J_p \int_0^\infty w(\lambda)\, d\lambda \text{ (watts/square foot)} , \tag{B.4}$$

where:

Ω_p = solid angle subtended by plaque (steradians)

A_p = area of plaque (square feet).

If the distance between the plaque and the lamp is d feet, we have

$$\Omega_p = \frac{A_p}{d^2} \tag{B.5}$$

and Eq. (B.4) reduces to

$$H = \frac{J_p}{d^2} \int_0^\infty w(\lambda)\, d\lambda \text{ (watts/square foot)} . \tag{B.6}$$

The reflectance of a magnesium oxide plaque is approximately $r = 1.0$ at 45 degrees, hence, we have the plaque radiance seen by the image intensifier as

$$N_p = \frac{Hr}{\pi} = \frac{J_p}{\pi d^2} \int_0^\infty w(\lambda)\, d\lambda \text{ (watts/square foot/steradian)} . \tag{B.7}$$

The photometer indication caused by the image intensifier viewing the plaque is

$$i_p = g\Omega_p A_L S_{20} \frac{J_p}{\pi d^2} \int_0^\infty \sigma(\lambda) \cdot w(\lambda)\, d\lambda \text{ (amperes)} . \tag{B.8}$$

Considering the ratio of i_{cw} to i_p from Eq. (B.2) and (B.8) one obtains:

$$\frac{i_{cw}}{i_p} = \frac{g\Omega_{II} A_L S_{20} N_w \int_0^\infty n(\lambda) \cdot \sigma(\lambda)\, d\lambda}{g\Omega_p A_L S_{20} \frac{J_p}{\pi d^2} \int_0^\infty \sigma(\lambda) \cdot w(\lambda)\, d\lambda} . \tag{B.9}$$

Since the plaque overfills the field of view of the image intensifier, Ω_p, the solid angle subtended by the plaque as shown in Fig. B-1 is effectively Ω_{II}, i.e., $\Omega_p = \Omega_{II}$. So

$$\frac{i_{cw}}{i_p} = \frac{\pi N_w d^2 \int_0^\infty n(\lambda) \cdot \sigma(\lambda)\, d\lambda}{J_p \int_0^\infty \sigma(\lambda) \cdot w(\lambda)\, d\lambda} . \tag{B.10}$$

By definition the effective radiance of the Cube wall in terms of the S-20 cathode responsivity of the image intensifier is

$$N_{cw}(S20) = N_w \int_0^\infty n(\lambda) \cdot \sigma(\lambda)\, d\lambda \text{ (watts/square foot/steradian)} . \tag{B.11}$$

It is the $N_{cw}(S20)$ portion of the total spectral radiance of the Cube wall that makes up the S-20 watts referred to in Eq. (B.2), i.e.,

$$W(S20) = \Omega_{II} A_L N_{cw}(S20) \text{ (watts)} . \tag{B.12}$$

Using Eq. (B.10) and(B.11) we obtain

$$N_{cw}(S20) = \frac{J_p i_{cw}}{\pi d^2 i_p} \int_0^\infty \sigma(\lambda) \cdot w(\lambda)\, d\lambda \text{ (watts/square foot/steradian)} . \tag{B.13}$$

Two integral evaluations germane to the solution of Eq. (B.13) are the following*:

(a)
$$\frac{\int_0^\infty \sigma(\lambda) \cdot w(\lambda)\, d\lambda}{\int_0^{1200} w(\lambda)\, d\lambda} = 0.110$$

and

(b)
$$\int_0^{1200} w(\lambda)\, d\lambda = 580 \text{ nm} .$$

Using (a) and (b) one obtains

(c)
$$\int_0^\infty \sigma(\lambda) \cdot w(\lambda)\, d\lambda = 0.110 \times 580 = 63.8 \text{ nm} .$$

* International Telephone and Telegraph (ITT) reference chart entitled "Typical Spectral Distribution Characteristics of Flux Sources, Filters, Windows, and Detectors."

Therefore, substituting (c) in Eq. (B.13) we have

$$N_{cw}(S20) = \frac{i_{cw}}{i_p} \frac{J_p}{\pi d^2} (63.8) \text{ (watts/square foot/steradian)} . \qquad \text{(B.14)}$$

Equation (B.14) could be evaluated at this point if the value of J_p were known since all other quantities are known. The J_p was not evaluated earlier in this development in order to avoid possible confusion. The natural jumping off place for evaluating J_p is Eq. (B.3) which is repeated here somewhat rearranged:

$$J_p = \frac{T_1 I}{680 \int_0^{\infty} \bar{y}(\lambda) \cdot w(\lambda)\, d\lambda} \text{ (watts/steradian/nanometer)} . \qquad \text{(B.15)}$$

Now again from the previously cited ITT chart we have

(d) $$\frac{\int_0^{\infty} \bar{y}(\lambda) \cdot w(\lambda)\, d\lambda}{\int_0^{1200} w(\lambda)\, d\lambda} = 0.071$$

and

(e) $$\int_0^{1200} w(\lambda)\, d\lambda = 580 \text{ nm.}$$

Therefore

(f) $$\int_0^{\infty} \bar{y}(\lambda) \cdot w(\lambda)\, d\lambda = 0.071 \times 580 = 41.3 \text{ nm.}$$

So using (f) and the known quantities $I = 9.09$ lm sr^{-1} (horizontal candlepower) and $T_1 = 0.126$ for the neutral density filter in Eq. (B.15), we obtain:

$$J_p = \frac{T_1 I}{680 \times 41.3} = \frac{9.09 \times 0.126}{680 \times 41.3} ,$$

yielding

$$J_p = 0.408 \times 10^{-4} \text{ W sr}^{-1} \text{ nm}^{-1} .$$

Returning to Eq. (B.14), the known quantities are listed below:

i_{cw} = 27 microamperes

i_p = 1.714×10^4 microamperes

J_p = 0.408×10^{-4} W sr^{-1} nm^{-1}

(63.8) = 63.8 nanometers

d = 9.85 feet.

Therefore, using these quantities results in

$$N_{cw}(S20) = \frac{i_{cw}}{i_p} \frac{J_p}{\pi d^2} (63.8) ,$$

$$= \frac{27 \times 0.408 \times 10^{-4} \times 63.8}{1.714 \times 10^4 \times \pi \times 9.85 \times 9.85} ,$$

and

$$N_{cw}(S20) = 1.35 \times 10^{-8} \text{ W ft}^{-2} \text{ sr}^{-1} .$$

This quantity is used directly in the theoretical predictions of Appendix C. With the aid of Eq. (B.11) the calculation of W(S20) is performed as indicated in Eq. (B.1).

B.6 EQUIVALENT SCENE LUMINANCE

The spectral character of the Cube wall radiance $n(\lambda)$ is not known nor is it necessary that it be known accurately in order to perform the work described in this report. Earlier in this appendix it is shown how the scene radiance can be determined without knowing the shape of $n(\lambda)$. The target radiance spectral character $t(\lambda)$ is probably somewhat different from $n(\lambda)$ because of the difference in neutral density attenuation between the background and the target projection systems. This effect is compensated for by measuring target and background separately as described earlier in this appendix. Because the image intensifier is used as the measuring instrument its output is relative to effective S-20 watts, hence the contrast measured is "effective S-20 contrast." It will be remembered that the S-20 radiance was $N_{cw}(S20) = 1.35 \times 10^{-8}$ W ft^{-2} sr^{-1}.

It is of interest to know what luminance of known spectral character would give the equivalent of 1.35×10^{-8} W ft^{-2} sr^{-1} of S-20 radiance, that is, would cause the same number of photoelectrons to be emitted by the photocathode of the image intensifier. For this purpose assume that the scene and target spectral character are that of 2870 K tungsten and represented by $\mu(\lambda)$.

Then, as previously stated in Eq. (B.11),

$$N_{cw}(S20) = N_w \int_0^\infty \sigma(\lambda) \cdot \mu(\lambda)\, d\lambda \text{ (watts/square foot/steradian)} . \tag{B.16}$$

The luminance is

$$B(\bar{y}) = 680 N_w \int_0^\infty \bar{y}(\lambda) \cdot \mu(\lambda)\, d\lambda \text{ (lumens/square foot/steradian)} . \tag{B.17}$$

Combining Eq. (B.16) and (B.17) one obtains

$$B(\bar{y}) = 680 \cdot N_{cw}(S20) \frac{\int_0^\infty \bar{y}(\lambda) \cdot \mu(\lambda)\, d\lambda}{\int_0^\infty \sigma(\lambda) \cdot \mu(\lambda)\, d\lambda} \text{ (lumens/square foot/steradian)} . \tag{B.18}$$

It is understood, of course, that the S-20 radiometer used to perform the measurements implied in Eq. (B.16) and (B.17) is properly calibrated and filtered for each measurement.

Now using the ITT data we have:

$$\int_0^\infty \sigma(\lambda) \cdot \mu(\lambda)\, d\lambda = 0.110 \times 580 = 63.8 \text{ nm}$$

and

$$\int_0^\infty \bar{y}(\lambda) \cdot \mu(\lambda)\, d\lambda = 0.071 \times 580 = 41.2 \text{ nm}.$$

So

$$B(\bar{y}) = 680 \times 1.35 \times 10^{-8} \times 41.2/63.8 = 5.93 \times 10^{-6} \text{ lm ft}^{-2} \text{ sr}^{-1}$$

or

$$B(\bar{y}) = 1.86 \times 10^{-5} \text{ ft-L}.$$

Hence a 2870K source of luminance equalling 5.93×10^{-6} lm ft^{-2} sr^{-1} would give the same effective photocathode irradiance as the Cube wall radiance $N_{cw}(S20) = 1.35 \times 10^{-8}$ W ft^{-2} sr^{-1} of spectral character $n(\lambda)$.

APPENDIX C. THEORETICAL DEVELOPMENT OF EQUATIONS FOR THE IDEAL DETECTOR

To provide an idea of the effectiveness of the image intensifier a set of theoretical alpha-contrast curves was computed. The theoretical basis for these computations is derived in this appendix.

C.1 SIGNAL-TO-NOISE RATIOS

As a first step the signal-to-noise ratios must be computed. It is assumed that the ideal detector employed is capable of performing optimum filtering, that is, the spatial characteristic of the filter matches the spatial characteristic of the target. The detector sensitivity, S, is given in terms of quantum efficiency, Q. Its temporal bandpass is Δf. Figure C-1 illustrates the geometry.

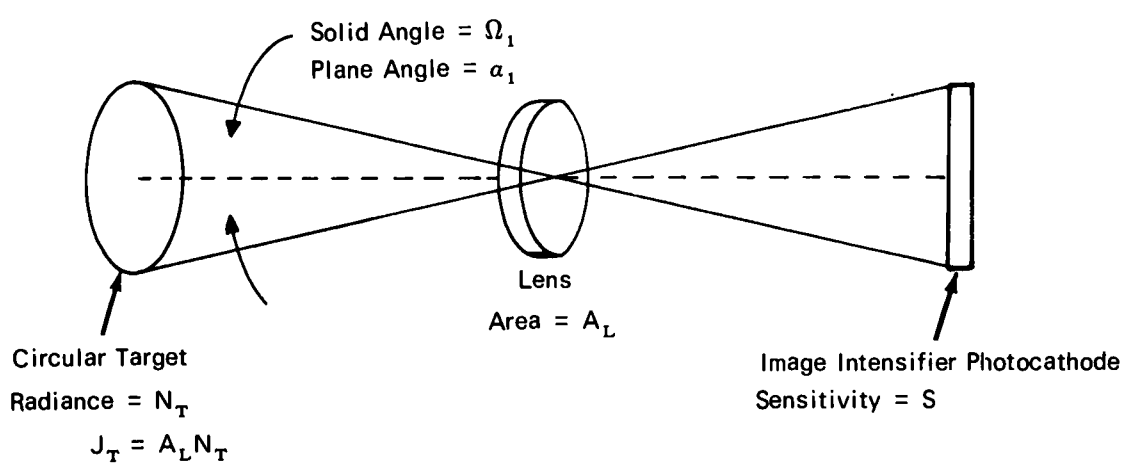

Fig. C-1. Target and Detector Geometry.

The functions shown in Fig. C-2 through C-5 were initially generated on the IBM System 360/44 computer at the Visibility Laboratory by means of the unique image processing software system developed at the Laboratory.[7] They were then displayed and photographed automatically on the refresh display associated with that system.

Figure C-2 illustrates the pertinent characteristics of the noise, signal, and optimum filter where the modulation transfer function (MTF) of the image intensifier is flat. Note in Fig. C-2 that the spatial domain figures represent cuts through right circular cylinders.

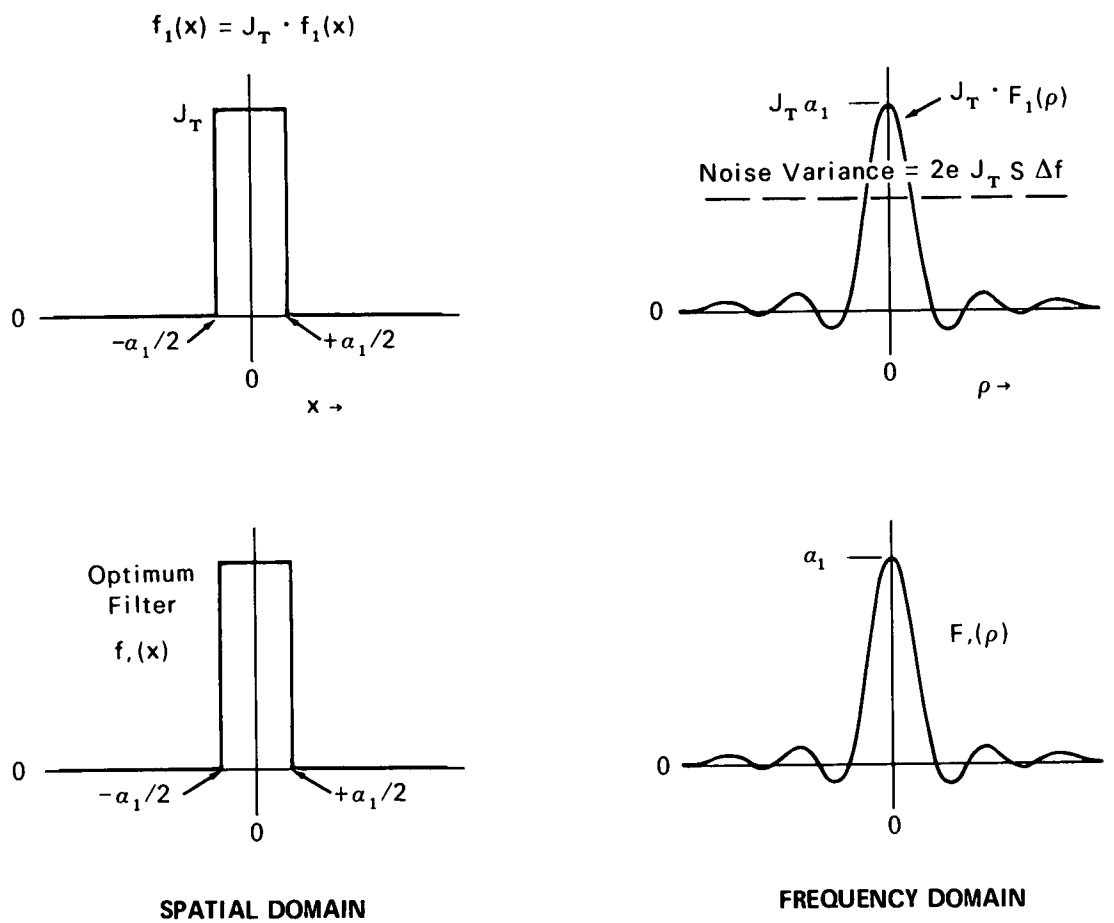

Fig. C-2. Domain Diagram With Target.

The peak signal current from the image intensifier photocathode, i_s, equals the product of the cathode sensitivity and the peak value of the convolution of the signal, f(x), and filter, $f_1(x)$:

$$\hat{i}_s = S \cdot f(x) * f_1(x) = J_T S \int_0^{\alpha_1/2} f_1^2(x) \cdot 2\pi x \, dx \, , \tag{C.1}$$

which reduces to

$$\hat{i}_s = \frac{J_T S \cdot \pi \alpha_1^2}{4} = J_T S \, \Omega_1 \, , \tag{C.2}$$

since

$$\frac{\pi \alpha_1^2}{4} = \Omega_1 \quad \text{for small } \alpha_1 (\alpha_1 \text{ in radians}) . \tag{C.3}$$

The relationship of i_s to the quadratic content of the filter can be illustrated by the application of Parseval's Theorem:

$$2\pi J_T S \int_0^{\alpha_1/2} x \, f_1(x)^2 \, dx = 2\pi J_T S \int_{-\infty}^{\infty} \rho |F_1(\rho)|^2 \, d\rho = J_T S \Omega_1 \, , \tag{C.4}$$

therefore

$$2\pi \int_{-\infty}^{\infty} \rho |F_1(\rho)|^2 \, d\rho = \Omega_1 \, . \tag{C.5}$$

But in Eq. (C.4),

$$2\pi \int_{-\infty}^{\infty} \rho |F_1(\rho)|^2 \, d\rho$$

is the quadratic content, $(QC)_1$, of the filter which in this special case of unity MTF equals the target solid angle. Hence,

$$\hat{i}_S = J_T S(QC)_1 \ . \tag{C.6}$$

The total noise variance is obtained by integrating the product of the filter power spectrum and the unfiltered noise power:

$$\sigma_S^2 = 2eJ_T S\Delta f 2\pi \int_{-\infty}^{\infty} \rho |F_1(\rho)|^2 \, d\rho \ , \tag{C.7}$$

$$\sigma_S^2 = 2eJ_T S\Delta f (QC)_1 \ , \tag{C.8}$$

and

$$\frac{\hat{i}_S}{\sigma_S} = \sqrt{\frac{J_T S}{2e\Delta f}} \cdot \sqrt{(QC)_1} \ . \tag{C.9}$$

If only background radiance is present, as is the case in those presentations devoid of a target, the above target spectrum can be replaced by an impulse function of value J_B. See Fig. C-3. Here again the figure for the filter represents a cut through a right circular cylinder. The background current, i_B, is expressed in Eq. (C.10):

$$i_B = J_B \cdot S2\pi \int_{-\infty}^{\infty} \rho |F_1(\rho)|^2 \, d\rho = J_B S(QC)_1 \ . \tag{C.10}$$

The background noise variance is

$$\sigma_B^2 = 2eJ_B S\Delta f (QC)_1 \tag{C.11}$$

and

$$\frac{i_B}{\sigma_B} = \sqrt{J_B S/2e\Delta f} \cdot \sqrt{(QC)_1} \ . \tag{C.12}$$

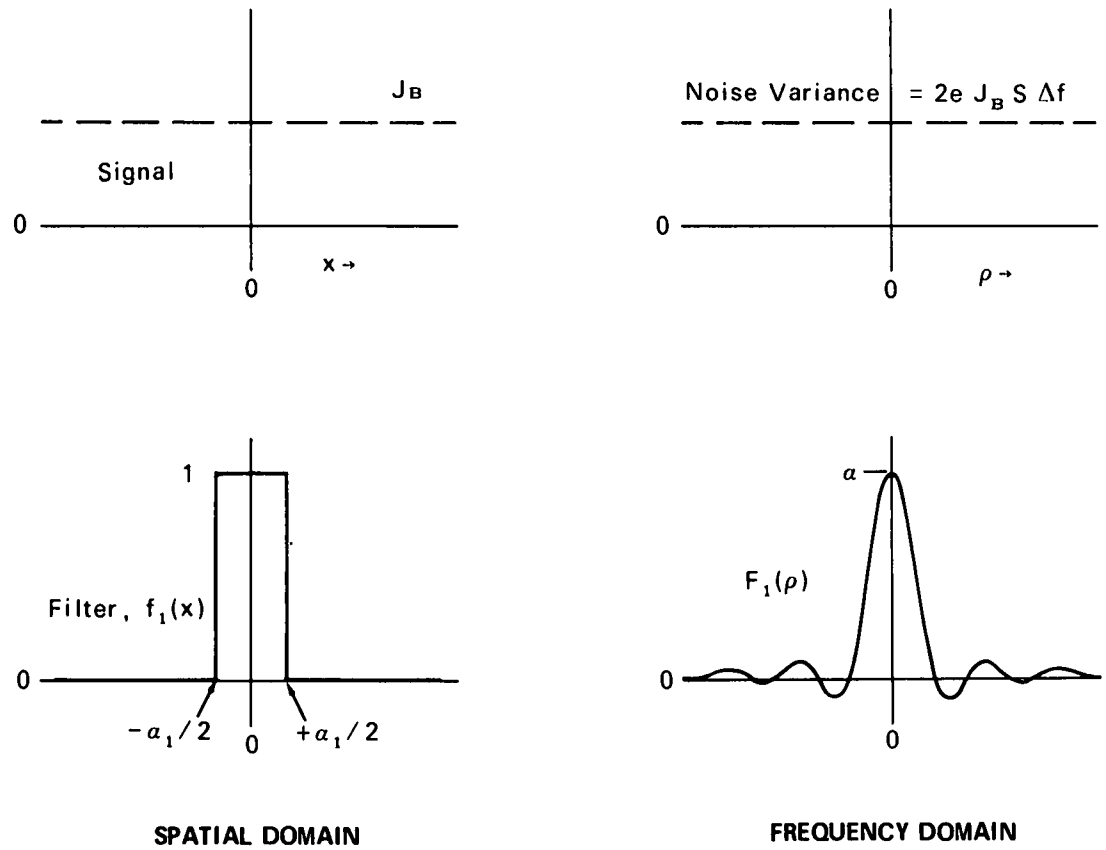

Fig. C-3. Domain Diagram Without Target.

The form of the MTF as plotted from the manufacturer's data (see Appendix A for resolution) was found to closely fit a Gaussian function representable by ϵ^{-ks^2}, where s is normalized spatial frequency, k = 10.1 is a constant, and ϵ is 2.718 or the natural base. If the MTF of the image intensifier is considered, the target signal spectrum is modified by this characteristic. Consequently, the ideal filter characteristic must be correspondingly altered. Figure C-4 illustrates this for the case previously shown in Figure C-2.

The relationship between $F_2(\rho)$ and $F_1(\rho)$ is simply

$$F_2(\rho) = \text{MTF} \cdot F_1(\rho) \ , \qquad \text{(C.13)}$$

where $f_2(x)$ and $F_2(\rho)$ are transform pairs.

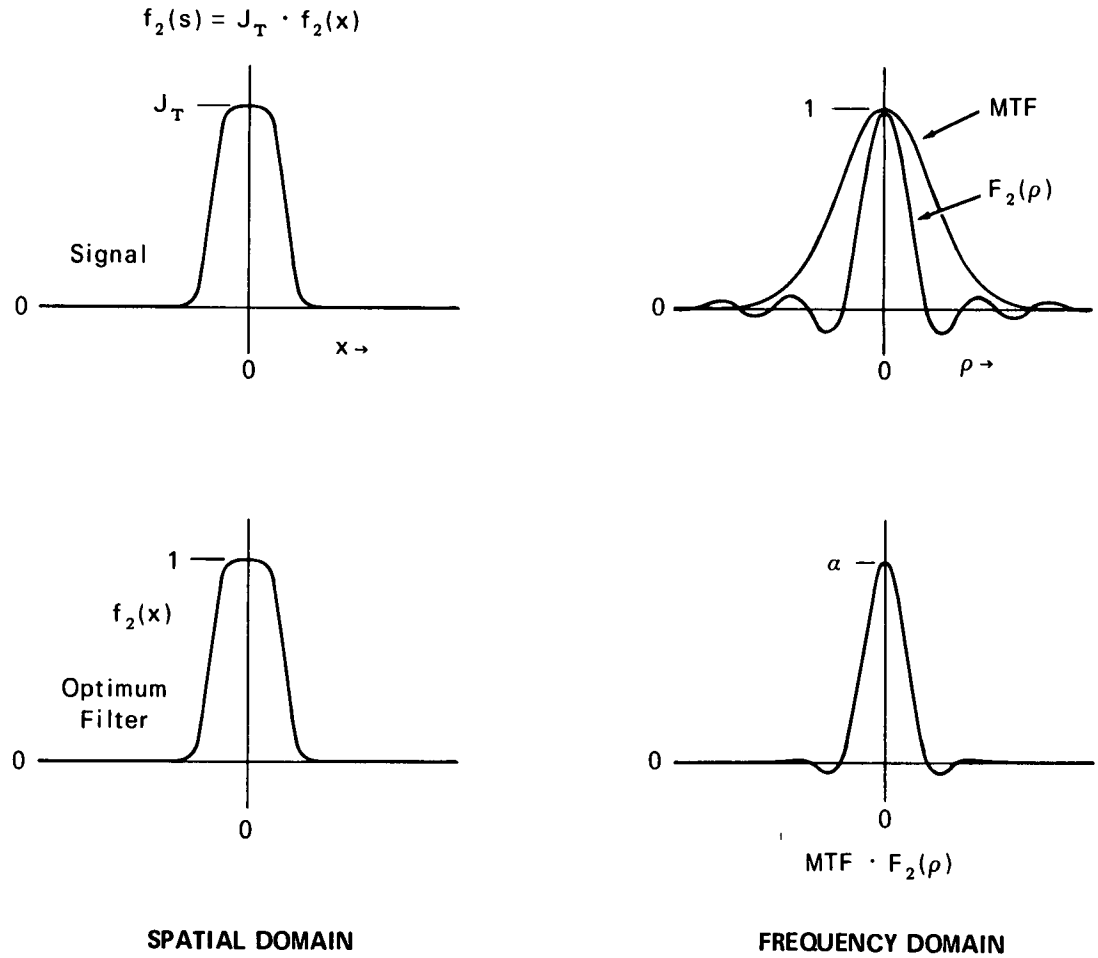

Fig. C-4. Domain Diagram Showing Effective MTF.

As before,

$$\frac{\hat{i}_s}{\sigma_s} = \sqrt{\frac{J_T S}{2e\Delta f}} \cdot \sqrt{(QC)_2} \quad . \tag{C.14}$$

In practice, the signal-to-noise ratios for a unity MTF are computed realizing that $(QC)_1$ is scaled to Ω_1. The signal-to-noise ratios for the actual MTF are obtained by computing

$$\frac{(QC)_2}{(QC)_1} = r \quad . \tag{C.15}$$

The $(QC)_2$ can be thought of as equivalent to an effective solid angle $\Omega_2 = \pi/4\ (\alpha_2^2)$:

$$(QC)_2 = \frac{\pi}{4}\alpha_2^2 = r\,(QC)_1 = r\,\frac{\pi}{4}\alpha_1^2 \ . \tag{C.16}$$

Therefore,

$$\alpha_2 = \sqrt{r\alpha_1} \ . \tag{C.17}$$

Once the alpha-contrast curves are plotted for a given quantum efficiency and a unity MTF, they can be adjusted for any MTF simply by modifying α by the square root of the quadratic content ratio.

To express J_T in the contrast form,

$$C = \frac{N_T}{N_B} - 1, \quad N_T = (C+1)N_B \ . \tag{C.18}$$

Therefore,

$$J_T = A_L(C+1)N_B \ . \tag{C.19}$$

It is instructive to observe the form of the equations for an MTF not equal to a constant for targets of very small angular subtense, i.e., targets not resolved by the image intensifier system. Figure C-5 illustrates the concepts involved for a target of 2-minute angular subtense.

Here we have

$$\hat{i}_S = S \cdot J_T \ \frac{\pi}{4}\ \alpha^2 f_3(x) * f_3(x) = S \cdot J_T \ \frac{\pi}{4}\ \alpha^2 \int_{-\infty}^{\infty} |F_3(\rho)|^2\, 2\pi\rho\, d\rho \tag{C.20}$$

so that

$$\hat{i}_S = SJ_T \ \frac{\pi}{4}\ \alpha^2 (QC) \ . \tag{C.21}$$

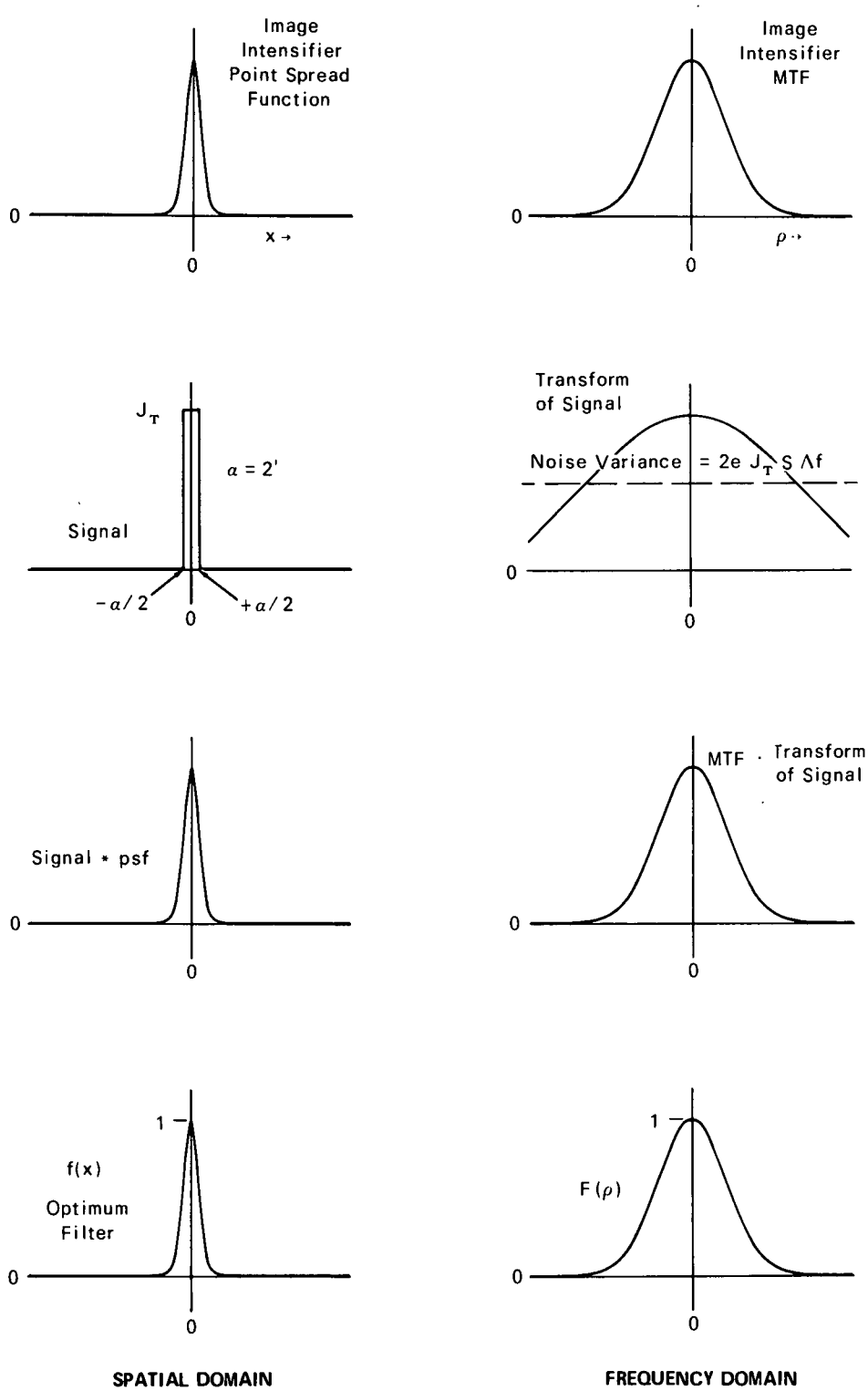

Fig. C-5. Domain Diagram for Unresolved Target.

Also,

$$\sigma_n^2 = 2eJ_T S\Delta f \int_{-\infty}^{\infty} |F_3(\rho)|^2 \, 2\pi\rho \, d\rho \tag{C.22}$$

and

$$\sigma_n = \sqrt{2eJ_T S\Delta f(QC)}, \quad \sigma_B = \sqrt{2eJ_B S\Delta f(QC)} \ . \tag{C.23}$$

Defining the signal-to-noise ratio as

$$\frac{S}{N} = \frac{\hat{i}_S - i_B}{\sigma_B} \ , \tag{C.24}$$

we have

$$\frac{S}{N} = \frac{SJ_T \ \frac{\pi}{4} \ \alpha^2(QC) - SJ_B \ \frac{\pi}{4} \ \alpha^2(QC)}{\sqrt{2eJ_B S\Delta f(QC)}} \ . \tag{C.25}$$

Since

$$C = \frac{J_T - J_B}{J_B} \ , \tag{C.26}$$

then

$$\frac{S}{N} = \frac{SCJ_B \ \frac{\pi}{4} \ \alpha^2(QC)}{\sqrt{2eJ_B S\Delta f(QC)}} \tag{C.27}$$

or

$$\frac{S}{N} = C\alpha^2 \sqrt{\frac{(\pi/4)^2 S J_B}{2e\Delta f}} \cdot \sqrt{(QC)} \quad . \tag{C.28}$$

So $C\alpha^2$ is a constant for small targets unresolved by the image intensifier system and the $\sqrt{(QC)}$ is simply a constant related to the MTF.

C.2 PROBABILITY FUNCTIONS

In this experiment, the existence of two events per trial is required to determine the incremental probability of a correct decision.[8] Let us assume that during the presentation interval when a target is present (Section 2.2 ibid) the photocathode current is Z (event 1). In order to yield a correct decision, the photocathode current in the remaining three intervals must be less than Z (event 2).

The probability of event 1 occurring is

$$P_1 = \frac{1}{\sqrt{2\pi}\sigma_S} \int_{-\infty}^{z} \exp - \frac{(Z - i_S)^2}{2\sigma_S^2} \, dz. \tag{C.29}$$

Because the target is present, σ_S and i_S are used. The current can only be between the limits of Z and Z + dZ.

Correspondingly, the probability of event 2 occurring is

$$P_2 = \left[\frac{1}{\sqrt{2\pi}\sigma_B} \int_{-\infty}^{z} \exp - \frac{(x - i_B)^2}{2\sigma_B^2} \, dx \right]^3 \quad . \tag{C.30}$$

Here, σ_B and i_B are used because the target is not present. The Gaussian is integrated from $-\infty$ to Z because the current values in these intervals are less than Z. Finally, the expression is cubed because the current must be less than Z in all three intervals.

The differential probability of making a correct decision implies that both events 1 and 2 occur:

$$dP = \frac{1}{\sqrt{2\pi}\sigma_S} \exp - \frac{(Z-i_S)^2}{2\sigma_S^2} \left[\frac{1}{\sqrt{2\pi}\sigma_B} \int_{-\infty}^{z} \exp - \frac{(x-i_B)^2}{2\sigma_B^2} \, dx \right]^3 dz \, . \qquad (C.31)$$

Since Z can take on all possible values, one must integrate over the range of Z to obtain the total probability of making a correct decision. Thus

$$P = \frac{1}{\sqrt{2\pi}\sigma_S} \int_{-\infty}^{\infty} \exp - \frac{(Z-i_S)^2}{2\sigma_S^2} \left[\frac{1}{\sqrt{2\pi}\sigma_B} \int_{-\infty}^{z} \exp - \frac{(x-i_B)^2}{2\sigma_B^2} \, dx \right]^3 dz \, . \qquad (C.32)$$

Using this equation one can calculate the performance of a detector capable of ideal filtering when presented with the psychophysics task.

By making the substitutions of

$$u = \frac{Z - i_S}{\sigma_S} \, , \; v = \frac{x - i_B}{\sigma_B} \, , \qquad (C.33)$$

it can be seen that the probability of making the correct decision is a function of the target and background signal-to-noise ratios:

$$P = \frac{1}{\sqrt{2\pi}} \int_{-\infty}^{\infty} \exp - \frac{u^2}{2} \left[\frac{1}{\sqrt{2\pi}} \int_{-\infty}^{(u\sigma_S + i_S - i_B)/\sigma_B} \exp - \frac{v^2}{2} \, dv \right]^3 du \, . \qquad (C.34)$$

Substituting from the previously derived Eq. (C.23) and (C.24) for the currents and standard deviations and utilizing the discussion relating to Eq. (C.15) and (C.16) results in the following form for the upper limit:

$$U.L. = u\sqrt{C+1} + C\alpha \sqrt{\frac{\pi}{4} \frac{N(S20)\, A_L\, S}{2e\Delta f}} \, . \qquad (C.35)$$

In this form, $P(\alpha, C)$ is represented as a function of two normal distributions both having unity standard deviation and zero mean. For a single (α, C) pair, one increment of the discretized integral is

$$\Delta P = \frac{1}{\sqrt{2\pi}} \exp - \frac{u^2}{2} \left[\frac{1}{\sqrt{2\pi}} \int_{-\infty}^{u \sqrt{C+1} + C\alpha K} \exp - \frac{v^2}{2} \, dv \right]^3 \Delta u , \qquad (C.36)$$

where

$$w = C\alpha \frac{\pi}{4} \frac{N(S20) A_L S}{2e\Delta f}$$

A program to compute $P(\alpha, C)$ was written for the IBM System 360/44 computer at the Visibility Laboratory. One additional parameter, Q, the quantum efficiency of the photocathode, was treated as a variable ranging from 1.0 to 0.01. Thus several families of sigmoid curves were generated. The variable S in the preceding equations can be thought of as the product of the inherent cathode sensitivity, $S' = 0.3$ amperes watt^{-1}, and the quantum efficiency of the photocathode, $S = S' Q$. Figure 3-3, repeated here for reader convenience as Fig. C-6, shows the computational results when the quantum efficiency of the photocathode is 1.0. From these curves the (α, C) pairs for $P = 0.50$ form the straight line labeled $Q = 1.0$ on Fig. 3-4.

When the contrast is zero, the limit of the second integral is simply u and $P = 0.25$. This result satisfies the concept of a correct guess by chance in a forced-choice experiment containing four time intervals.

Figure 3-1, repeated here as Fig. C-7, shows the results of one typical observer participating in the psychophysics experiment. For target sizes greater than about 30 minutes, the empirical ogives in Fig. C-7 tend to merge as the minimum contrast detection capability of the eye is approached. The (α, C) pairs at $P = 0.50$ form the curve in Fig. 3-4 labeled Empirical Results.

When the value of C is $\ll 1.0$, the upper limit, Eq. (C.35), reduces to $u + w$, where

$$w = C\alpha \frac{\pi N(S20) A_L S}{4e2\Delta f} , \qquad (C.37)$$

and P can therefore be specified uniquely as a function of w:

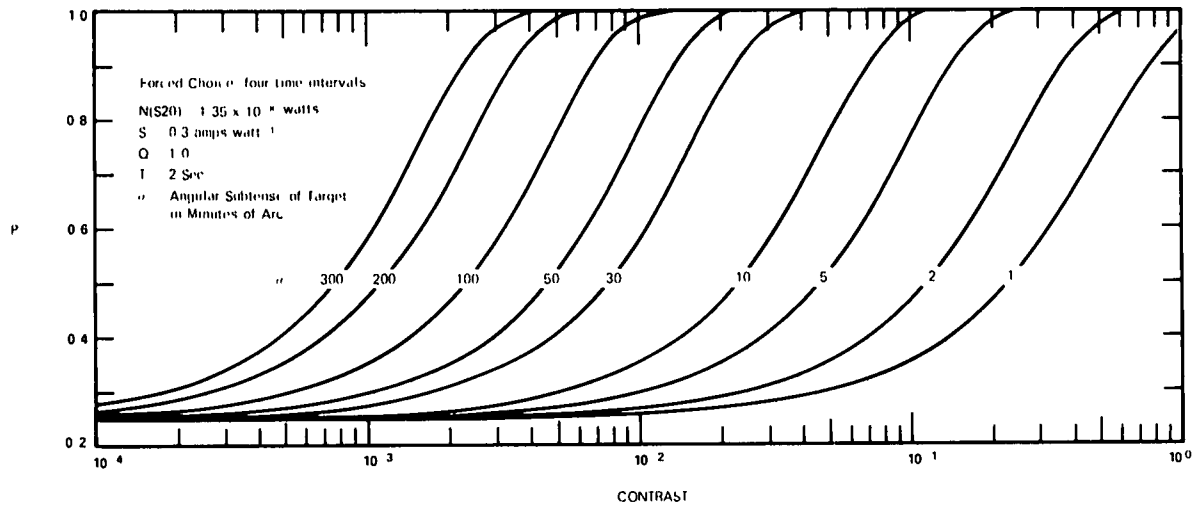

Fig. C-6. Probability of Correct Decision by Ideal Detector.

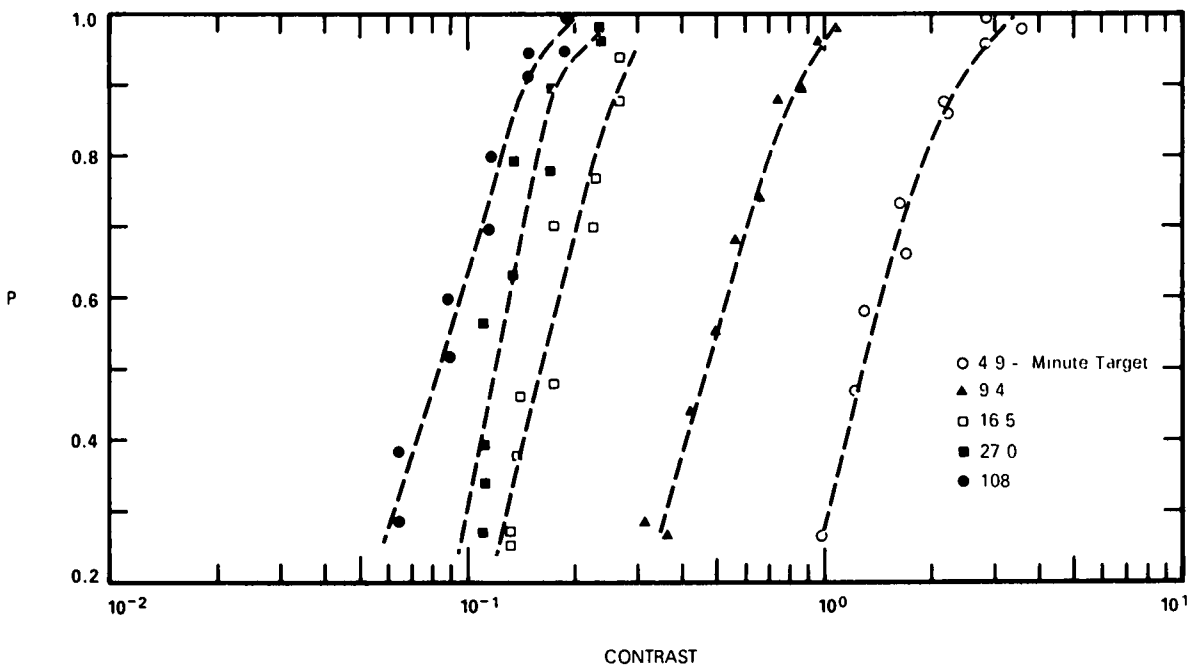

Fig. C-7. Psychophysics Results for One Observer.

$$P(w) = \frac{1}{\sqrt{2\pi}} \int_{-\infty}^{\infty} \exp\left(-\frac{u^2}{2}\right) \left[\frac{1}{\sqrt{2\pi}} \int_{-\infty}^{u+w} \exp\left(-\frac{v^2}{2}\right) dv \right]^3 du \,. \tag{C.38}$$

This function is shown in Fig. C-8.

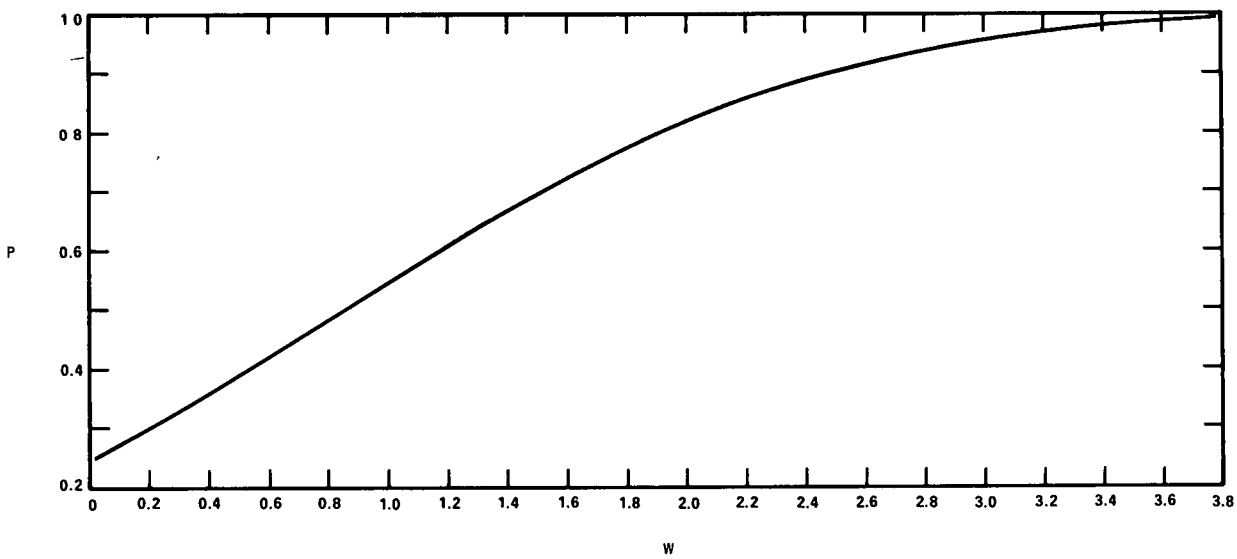

Fig. C-8. Probability Approximation for Contrast Much Less Than 1.0.

Thus, for any particular probability, e.g., 0.50, the corresponding w is known and an (α, C) curve for the ideal detector can be generated by assigning an α and computing the required C from Eq. (C.37). One can see that any (α, C) curve for the ideal detector (Fig. 3-4) will have a unity slope as long as the following conditions are met:

1. $C \ll 1.0$ (Examination of the ideal detector curves in Fig. 3-4 implies that the straight line approximation is valid for $C < 0.3$.)

2. The number of electrons, N_e, corresponding to the signal current is large enough so that Gaussian statistics apply. The N_e can be computed from

$$N_e = \frac{i_B \Delta t}{e} \,, \tag{C.39}$$

where

$$\Delta t = \frac{1}{2\Delta f} .$$

3. The resolution of the detector is not a factor.

Eventually, for small targets well below the resolution of the image intensifier, the relationship $C\alpha^2$ equals a constant hold, resulting in a slope of $-1/2$ on a logarithmic plot. This follows from Eq. (C.28) which shows, for very small targets, that

$$\frac{\hat{i}_S - i_B}{\sigma_B} = C\alpha^2 \sqrt{\frac{(\pi/4)^2 S J_B}{2e\Delta f}} \cdot \sqrt{(QC)} .$$

The simplification described for $C \ll 1.0$ is extremely useful when considering changes in the various parameters which describe the characteristics of the ideal detector. Typical values used in the theoretical computation were:

$$N(S20) = 1.35 \times 10^{-8} \text{ W ft}^{-2} \text{ sr}^{-1}$$

$$2\Delta f = 0.5 \text{ sec}^{-1}$$

$$A_L = 0.004 \text{ ft}^2 \text{ (Bausch and Lomb Baltar, f/2.3, 50 millimeters)}$$

$$e = 1.6 \times 10^{-19} \text{ coulombs electron}^{-1}$$

$$\left.\begin{aligned} S' &= 0.3 \text{ amp watt}^{-1} \\ Q &= 1.0. \end{aligned}\right\} S = 0.3 \text{ amp watt}^{-1}$$

To verify the u+w concept for $C \ll 1.0$, one can choose some (α, C) pair from the precise computation of P (Eq. C.34). For example, from the liminal curve $Q = 1.0$, $T = 2.0$ at $\alpha = 100$ minutes of arc, $C = 0.0023$. Then

$$w = C\alpha \sqrt{\frac{\pi N(S20) A_L S}{4e2\Delta f}} \cdot 8.46 \times 10^{-8} = 0.843 .$$

The constant 8.46×10^{-8} is the conversion from radians^2 to minutes. For $P(w) = 0.5$ from Fig. C-8, we obtain $w = 0.84$.

Typical signal and noise values associated with the ideal detector at $P = 0.50$ are given in Table C-1 below.

Table C-1. Typical Values from Theoretical Study

Parameters	Values						Units
Q	1.0	1.0	0.2	0.2	0.2	0.2	–
T	2.0	2.0	2.0	2.0	0.2	0.1	seconds
α	5.0	30.0	5.0	30.0	10.0	100.0	minutes of arc
C	0.045	0.0075	0.102	0.0172	0.162	0.023	–
S	0.3	0.3	0.06	0.06	0.06	0.06	amperes/watt
i_B	2.68E-17	9.64E-16	5.36E-18	1.93E-16	2.14E-17	2.14E-15	amperes
i_S	2.80E-17	9.71E-16	5.90E-18	1.96E-16	2.49E-17	2.19E-15	amperes
σ_B	1.46E-18	8.78E-18	6.54E-19	3.93E-18	4.14E-18	5.85E-17	–
σ_S	1.50E-18	8.81E-18	6.87E-19	3.96E-18	4.46E-18	5.92E-17	–
N_e	3.35E02	1.20E04	6.69E01	2.41E03	2.68E01	1.34E03	electrons
S/N	0.82	0.82	0.83	0.84	0.84	0.84	–

REFERENCES

1. Taylor, John H., "Practice Effects in the Performance of a Simple Visual Discrimination Task by Initially Naive Observers," SIO Ref. 62-21 (October 1962).

2. Blackwell, H. Richard, "Psychophysical Thresholds: Experimental Studies of Methods of Measurement," Univ. of Mich. Eng. Research Inst., Bull. No. 36 (1953), p. 227.

3. Richardson, William H., "An Adaptation of the Method of Probit Analysis to Psychophysical Threshold Data," SIO Ref. 60-47 (June 1960).

4. Richardson, William H., "A Study of the Factors Affecting the Sighting of Surface Vessels from Aircraft," SIO Ref. 62-13 (June 1962), p. 8.

5. Anon., "Visibility of Targets (Record of Research)," Vol. I-V, The Louis Comfort Tiffany Foundation, NDRC Div. 16-250-M2 (March 1943 – September 1945).

6. Blackwell, H. Richard, Pritchard, B. S., and Ohmart, J. G., "Automatic Apparatus for Stimulus Presentation and Recording in Visual Threshold Experiments," J. Opt. Soc. Am. **44**, 322-326 (1954).

7. McGlamery, Benjamin L., Myers, Madison L., Ensminger, Richard L., Howarth, Robert F., "Progress in Image Processing Techniques and Equipment," SIO Ref. 69-28 (November 1969).

8. Harris, James L., Sr., "Studies of Mathematical Models of Visual Performance Capability," Report 1, Bureau of Ships Contract No. NObs-86012 (January 1963).

UNCLASSIFIED
Security Classification

DOCUMENT CONTROL DATA - R&D

(Security classification of title, body of abstract and indexing annotation must be entered when the overall report is classified)

1 ORIGINATING ACTIVITY *(Corporate author)*
Visibility Laboratory
University of California
San Diego, California 92152

2a. REPORT SECURITY CLASSIFICATION
UNCLASSIFIED

2b. GROUP

3 REPORT TITLE

IMAGE INTENSIFIER SYSTEM DETECTION EXPERIMENT

4 DESCRIPTIVE NOTES *(Type of report and inclusive dates)*
Technical Report, March through May 1970

5 AUTHOR(S) *(Last name, first name, initial)*
Ensminger, Richard L.
Howarth, Robert F.
Shaules, Alma L.

6 REPORT DATE	7a. TOTAL NO OF PAGES	7b NO OF REFS
June 1972	43	8

8a. CONTRACT OR GRANT NO	9a. ORIGINATOR'S REPORT NUMBER(S)
N00024-68-C-1100	SIO Ref. 72-60
b.	
c.	9b. OTHER REPORT NO(S) *(Any other numbers that may be assigned this report)*
d.	

10 AVAILABILITY/LIMITATION NOTICES
Distribution limited to U.S. Government agencies only; Test and Evaluation; June 1970. Other requests for this document must be referred to Commander, Naval Ship Engineering Center, Code 6178C.03, Department of the Navy, Washington, D. C. 20360.

11 SUPPLEMENTARY NOTES	12 SPONSORING MILITARY ACTIVITY
	U. S. Naval Ship Systems Command Department of the Navy Washington, D. C. 20360

13 ABSTRACT

This report describes experiments to evaluate the efficiency of human information extraction from an image intensifier system. A detection experiment was run with circular targets. The variables of the experiment were the angular size of the targets and the contrast of the targets. The experimental data are compared with calculations of the performance that would be achieved if the observer extracted all information collected by the image intensifier system.

DD FORM 1 JAN 64 1473

UNCLASSIFIED
Security Classification

14 KEY WORDS	LINK A		LINK B		LINK C	
	ROLE	WT	ROLE		ROLE	WT
Night Vision						
Visual Thresholds						
Image Intensifier						
Cathode Ray Tube Displays						